Robust Control of a Wind Turbine Using Third Generation CRONE Control

Francisco Ravasco
fsravasco@gmail.com

Instituto Superior Técnico, Universidade de Lisboa, Lisboa, Portugal

November 2018

Abstract

This document focuses on the analysis, development and simulation of a fractional-complex third generation CRONE (French acronym for *Commande Robuste d'Ordre Non Entier*) controller for a new Darrieus VAWT prototype.

The prototype is studied, and its numerous dynamic models, proposed in previous works, are analysed. Previously acquired experimental data from the prototype is studied, and a new, more truthful TSR range is proposed. The CRONE control system design methodology is studied, and a controller is developed for the model that better describes the prototype's behaviour.

The model selected (nominal plant) is used to produce two additional models (extreme plants, 1 and 2), that introduce $\pm 20\%$ uncertainty in the nominal plant's transfer function coefficients. The CRONE controller is tested in simulation, when applied to each of the three plants, in different wind conditions, with and without the presence of turbulence. The controller's performance is presented and analysed, resorting to two metrics used in the literature: the *ITAE* and the *ISV*.

A set of sensors and actuators integrated with the *Arduino* platform, are proposed and built for the prototype, and two real tests are performed. One, to validate the TSR range proposed at the beginning of the document, and another, to assess the limitations imposed by the actuator in the prototype's TSR behaviour.

Keywords: Wind Energy; Darrieus Wind Turbines; Prototype; Control Strategy; Fractional Control; Third Generation CRONE Control

1. Introduction

Wind turbines are now considered one of the most conspicuous energy sources. Their development was hastened by an increasing demand for energy and by a growing awareness on environmental issues.

According to *GWEC*, the new installations in 2017 represented $52489\,\mathrm{MW}$, rising the global total installed wind capacity to $539123\,\mathrm{MW}$ [1]. According to the same source, wind power has faced a growth of over 2000% in installed power, over the last sixteen years.

Nowadays, the vast majority of wind turbines installed are Horizontal Axis Wind Turbines (HAWT). This implies that the energy is produced far from the final user, inducing more costs, as, due to the noise production and visual impact, this technology is not suited to urban environment. The solution may pass through Vertical Axis Wind Turbines (VAWT), resorting to a larger number of turbines spread over each city, producing decentralised electricity in a Smart Grid context. Even though they are behind HAWT in development and investment, VAWT present several advantages [2]:

- Insensitivity to yaw wind direction;
- Smaller number of components;
- Low sound emission;
- Ability to produce energy from wind in skewed flows;
- Capable of operating closer to the ground level;
- Generator position closer to the ground level, allowing for an easier maintenance.

A VAWT is classified into two different types: Darrieus and Savonius. The prototype studied in the present document is a curved blade Darrieus VAWT. It was developed and tested in [2–6]. Unlike Savonius VAWT, the Darrieus wind turbine, usually requires a start-up force to begin its movement.

In [4] the Darrieus wind turbine prototype is developed, featuring a new blade design that ensures its self-start capabilities. Numerous field tests are presented in [2], concluding that the new design guarantees a self-start for winds speeds starting at

$1.25\,\mathrm{m/s}$, exhibiting a stable behaviour under stress for winds up to $25\,\mathrm{m/s}$, maintaining a good performance. The integration of this new Darrieus VAWT in urban context is studied in [5], with the presentation of performance prediction models. The study includes self-start tests, noise production assessment, and predictions in different types of turbulent and unstable wind behaviours, that are common in urban areas. Theoretical models for the prototype are proposed in [6], along with different identified models. A PID controller and an LQR are developed and tested in simulation using the models previously developed. In the present document, the model with a greater fit to real data will be analysed, and used for the controller synthesis and simulation tests.

The CRONE control began being presented to the engineers community in [7], where the principles of the first generation CRONE controller were stated. The third generation was only present in [8]. This generation represents the generalisation of the first two approaches. Based on the complex non-integer derivation, the generalised template is defined, as an indifferent direction straight line segment. Then, a performance criterion is established to select an optimal template that ensures the robustness of the controller within its uncertainty domain.

More recently, a toolbox was developed by the CRONE research group, in Ref.[9] the toolbox for *Matlab* is presented along with a tutorial and a case study to simplify the usage among the engineer community.

The present document is organised as follows: In section 2 numerous considerations about the prototype are presented; the selected model is presented and analysed; the turbulent wind model to be used in simulation is presented; and the guidelines of the third generation CRONE control are stated. In section 3 an analysis on the model with the uncertainty domains is made; the controller objectives are stated; and the controller synthesis explained. In section 6 the results obtained in simulation are presented and the controller performance is evaluated. In section 7 the experimental setup is explained, and the sensors and actuators are described. Finally, section 9 outlines the conclusion.

2. Background

In this section, the prototype's technical specifications will be presented, as well as the selected model that describes the prototype. The turbulent wind model, that will be used in simulation, is described, and the guidelines for the third generation CRONE control are stated.

2.1. Prototype Considerations

Firstly, it is important to present the prototype's technical specifications, which are stated in Table 1. To assess the veracity of the models considered,

Table 1: Turbine's Specifications

PARAMETERS	SYMBOL	VALUE
$N^{o}\ of\ Blades$	Z	5
$Rotor\ Height\ [\mathrm{mm}]$	H	480
$Rotor\ Radius\ [\mathrm{mm}]$	r	173
$Blade\ Body\ Height\ [\mathrm{mm}]$	-	360
$Blade\ Profile\ Chord\ [\mathrm{mm}]$	c	53
$Moment\ of\ Inertia\ [\mathrm{kgm}^2]$	J_t	0.1

it is important to observe some real data from the prototype. In Figure 1 is presented real data collected in [2].

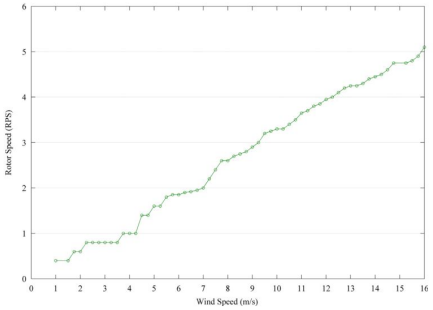

Figure 1: Real Prototype Data, Wind Speed vs Angular Speed, from [2]

The data presented was collected with the PMSG in open circuit, therefore it represents the higher $\frac{\omega_{[\mathrm{rad/s}]}}{v_{[\mathrm{m/s}]}}$ relation capable by this prototype. As this type of VAWT has a fixed pitch, it is expected that the rotor's angular speed to be directly proportional to the incoming wind speed. The data can be roughly described by (1):

$$\frac{\omega_{[rad/s]}}{v_{m/s}} = 2.04 \tag{1}$$

where ω is the rotor's angular speed, and v is the incoming wind speed.

Taking into account (1) as the maximum achievable by the prototype with this PMSG, and knowing that the tip speed ratio (TSR) is given by:

$$\lambda = \frac{\omega\, r}{v} \tag{2}$$

where r is the rotor radius, from Table 1. One can calculate the corresponding maximum TSR, given by:

$$\lambda_{max} = 2.04 \cdot r \approx 0.353 \tag{3}$$

The $C_P(\lambda)$ function proposed for the turbine in [2] is shown in Tigure 2. The fitted curve is given by:

$$C_P(\lambda) = -0.007365\,\lambda^2 + 0.1015\,\lambda + 0.002052 \tag{4}$$

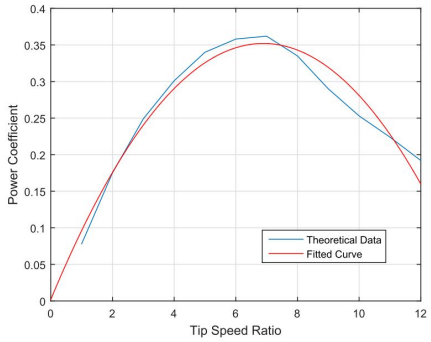

Figure 2: Power Coefficient (C_p) vs Tip Speed Ratio (λ) proposed in [2]

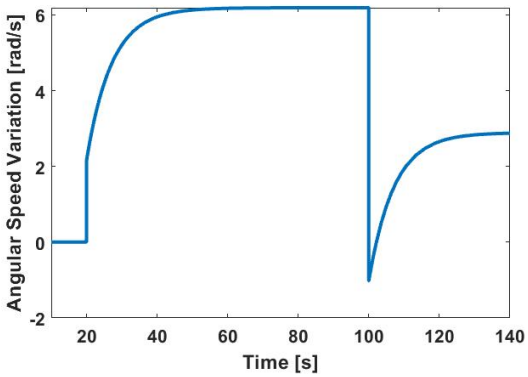

Figure 3: Multiple Input Single Output Response

The simulation that originated the theoretical relationship presented in Figure 2 considers a turbine with $4.6\,\mathrm{m}$ of height and $2\,\mathrm{m}$ of radius. Therefore, it is expected that the theoretical models built using (4) do not describe rigorously this prototype. This said, instead of using as reference the TSR value used in [6], which is impossible to reach, a plausible hypothetical value will be assumed as $\frac{2}{3}$ of the maximum TSR:

$$\lambda_{opt} = \frac{2}{3}\lambda_{max} \approx 0.2353 \tag{5}$$

This value will be used for simulation purposes in the remaining of this document.

2.2. Selected Model

Five models for the turbine were developed in [6]. These five models were analysed and the one obtained from MISO identification methods with free matrix entries, was the one that represented more accurately the prototype's behaviour. Therefore, this was the model selected to proceed with the controller synthesis.

The identified transfer function in [6] is given by:

$$\Delta\omega(s) = \frac{7131\,s + 2879.9}{s^2 + 13200\,s + 1861}\Delta v(s) + \frac{952\,s + 61.41}{s^2 + 13200\,s + 1861}\Delta Rc(s) \tag{6}$$

where the inputs $\Delta v(s)$ and $\Delta Rc(s)$ are the wind speed variation and the PMSG circuit load variation, respectively. And the output $\Delta\omega(s)$ is the rotor's angular speed variation. To observe the model reaction to both inputs, it was fed with a step input in the wind speed variation $\delta v = 4\,\mathrm{m/s}$ at $t = 20\,\mathrm{s}$. The load imposed resistance was kept at $\delta R_c = 0\,\Omega$ until $t = 100\,\mathrm{s}$, thereafter being changed for $\delta R_c = -100\Omega$. This model is a linear model around the working point $\overline{v} = 6\,\mathrm{m/s}$ and $\overline{R_c} = 136.6\,\Omega$ [6]. The model's response is presented in Figure 3. The model's response, is in line with what was said in [6].

The wind speed variation effect in the angular speed has much faster dynamics than the real prototype, resulting in an instant increase of $2\,\mathrm{rad/s}$ at $20\,\mathrm{s}$, a growth that should be gradual. Nonetheless, this is the model that describes better the prototype [6], and it will be used to synthesise the controllers and to simulate the prototype's behaviour.

2.3. Turbulent Wind Model

In cases such as the present one, the study of the wind behaviour around buildings and other man made formations assumes a role of extreme importance [10].

As it is impossible to avoid the turbulence present in the wind, the solution is to consider the atmospheric turbulence when developing wind powered systems. The model chosen to simulate this turbulence present in the wind, is given by [11]:

$$v = v_0\left[1 + \sum_k A_k\,\sin(\omega_k\,t)\right] \tag{7}$$

being k an index associated with the mechanical oscillation excited, A_k the amplitude of the k oscillation, and ω_k the frequency of the same oscillation. The mechanical oscillations are modelled by a frequency range between 0.1 and $10\,\mathrm{Hz}$, Table 2 presents these values [11].

Table 2: Mechanical Oscillations

Source	k	A_k	ω_k
$Assimetry$	1	0.01	ω_k
$TowerShadow$	2	0.08	$3\,\omega_k$
$Blades$	3	0.15	$9\,\pi$

2.4. Third Generation CRONE Control

The CRONE Control System Design (CSD) theory is based on the complex non integer derivation. It is a frequency domain approach that has been developed since the $1980s$. Three CRONE CSD methods have been developed sequentially,

extending the field of application of this control system. In all three methods, the controller is designed resorting to fractional order integro-diferentiation [12].

The main objective of this type of control is to ensure that the closed-loop gain or damping coefficient, or both, will never get beyond a certain value, even if some plant's parameter vary within a known range.

In third generation CRONE the Nichols locus is defined as a straight-line segment around frequency ω_{cg} for the nominal parametric state of the plant. From [8], the open loop transfer function is given by:

$$\beta(s) = \left(\cosh\left(b\frac{\pi}{2}\right)\right)^{\mathrm{sign(b)}} \left(\frac{\omega_{cg}}{s}\right)^{a} \left(\cos\left(b\,\ln\left(\frac{s}{\omega_{cg}}\right)\right)\right)^{-\mathrm{sign(b)}} \quad (8)$$

The real part a determines the phase location of the generalised template at frequency ω_{cg}, that is $-a\frac{\pi}{2}$, and the imaginary part b determines its angle to the vertical (Figure 4).

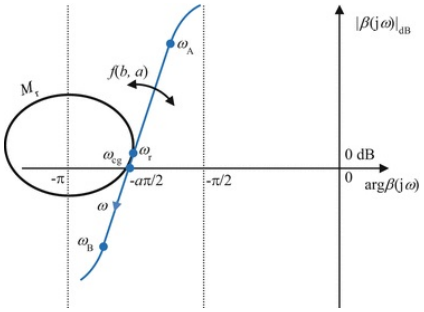

Figure 4: Generalised Template, from [12]

2.4.1 Optimal Template

When considering the uncertainty of the plant, one has to account for the variations such uncertainties will cause in the desired ressonant peak M_r, and minimise the influence of the plant's uncertainties to ensure stability.

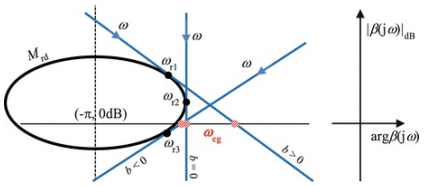

Figure 5: 3 Generalised Templates that Tangent a Given M-contour, from [12]

There is an indefinite number of generalised templates tangent to the desired M-contour for the nominal parametric state of the plant (Figure 5); from these, the Optimal Template is the one that minimises the M_r variations.

The optimal template is achieved resorting to a robustness-oriented cost function that minimises this overlapping. That function is given by [12]:

$$J = \sup_{\omega,G} |T(\mathrm{j}\omega)| - \mathrm{M_{rd}} \quad (9)$$

subject to a set of five frequency domain constraints, that can be found in [12].

Resorting to the CRONE Toolbox for Matlab, these principles will be applied in the development of a third generation CRONE controller for the plant.

3. Controller Development

3.1. Model Analysis

In this system there are two inputs and one output, as only the PMSG resistance (Rc) is controllable, the contribution from the wind velocity (v) to the output is treated as a disturbance that one can not predict. With this in mind, only the transfer function of the main process $\left(\frac{\Delta\omega(s)}{\Delta Rc(s)}\right)$ will be analysed for the controller synthesis. This transfer function is given by:

$$\frac{\Delta\omega(s)}{\Delta Rc(s)} = \frac{0.033\,(\frac{s}{0.0645}+1}{(\frac{s}{13200}+1)(\frac{s}{0.141}+1)} \quad (10)$$

For a better understanding of the system's characteristics a bode diagram is shown in Figure 6.

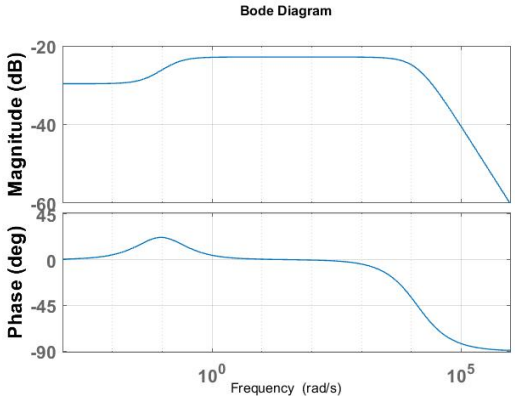

Figure 6: Bode Diagram

The system is stable in closed loop for all values of $K \geq 0$. The bode diagram of figure 6 shows that the system has infinite gain and phase margins .

As it has not been possible to acquire real data at the time the controller was developed, the uncertainty present in the model was assumed to be of $\pm 20\%$ in the plant's coefficients. The nominal plant's Nichols locus, with the uncertainty domains and the extreme plants, is presented in Figure 7. The extreme plants are useful to simulate the system's response in the extremes considered. The

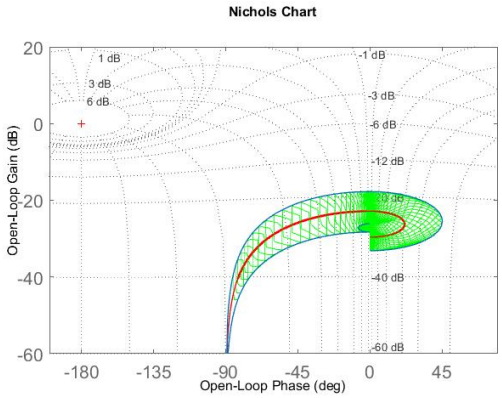

Figure 7: Green - Uncertainty Domains; Red - Nominal Plant; Blue - Extreme Plants

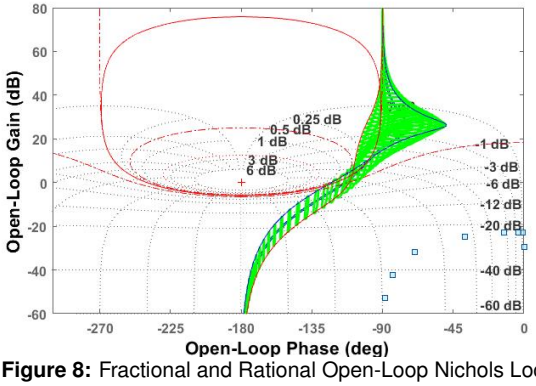

Figure 8: Fractional and Rational Open-Loop Nichols Locus

two extreme plants are given by:

$$\frac{\Delta\omega(s)}{\Delta Rc(s)} = \frac{1142\,s + 40.94}{s^2 + 8800\,s + 1861} \tag{11}$$

$$\frac{\Delta\omega(s)}{\Delta Rc(s)} = \frac{761.6\,s + 92.11}{s^2 + 19800\,s + 1861} \tag{12}$$

4. Control Objectives

The main objective of the control strategy is to maintain the turbine's efficiency at its maximum. This translates into trying to maintain the Tip Speed Ratio (λ) in a value that maximises the C_p, making use of the influence Rc has on ω, whatever the wind speed passing through the turbine. As stated before, it will be assumed for simulation purposes that the λ_{opt} for which C_p is maximum is $\lambda = 0.2353$.

The specifications proposed in [6] for the system's closed-loop step response were:

- $Maximum\,Overshoot:\ M_p \leq 20\%$
- $Settling\,Time:\ t_s[2\%] \leq 10s$

5. Third Generation CRONE Control System Design

For the design of the controller, the *CRONE CSD Toolbox for Matlab* was used. The Toolbox allows synthesizing any CRONE controller, from first to third generation, by setting the specifications in the software and adjusting the different sensitivity functions that characterise the system. After several modifications of the parameters and sensitivity functions, the Nichols locus obtained after applying the rational controller is shown in Figure 8.

6. Simulation Results & Controller Performance

6.1. Without Turbulence

The controller was firstly tested using a step as wind perturbation, neglecting the turbulence present in the wind, to assess the controlled closed-loop system's behaviour and the uncontrolled response in closed-loop ($C = 1$). In nature, the wind does not have an abrupt (*step-like*) behaviour. However, it is valid to admit that, if the system behaves accordingly with a step input disturbance, in the presence of smoother disturbances its performance should be of higher quality.

For this test, the wind is kept at its nominal value, assumed to be $v = 6\ m/s$, and at $t = 30s$ the disturbance is simulated as a step $\Delta v = 4\ m/s$. For $t \geq 10s$ the wind velocity is kept at its final value $v = 10\ m/s$.

Firstly, for comparison purposes, this test was performed in closed-loop without controller ($C = 1$), for the nominal plant and both extreme plants. The results are presented in Figure 9. The difference between the nominal and extreme plant's response is small. This is due to the fact that the uncertainty was only introduced in the transfer function from ΔRc to $\Delta\omega(s)$, and this transfer function has a low open loop gain (Figure 7).

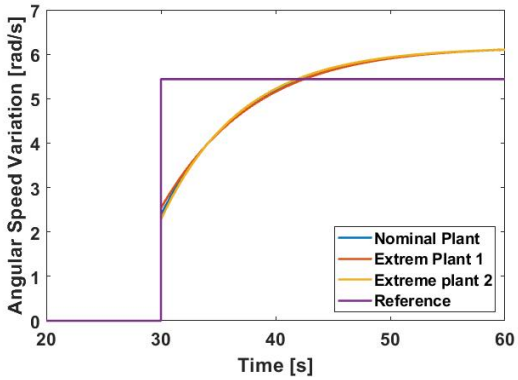

Figure 9: Closed-loop Response ($C = 1$)

The same test was performed for the controlled nominal plant, and for both extreme plants, the result is presented in the Figure 10. The angular velocity variation follows the reference needed to maintain the TSR at the optimum value, all three plants present a settling time lower than $10\,s$ and an overshoot of less than 10%, fulfilling the specifications. The control effort presented in figure 11, shows that the load imposed resistance reaches values of around $200\,\Omega$, for the extreme plant 2.

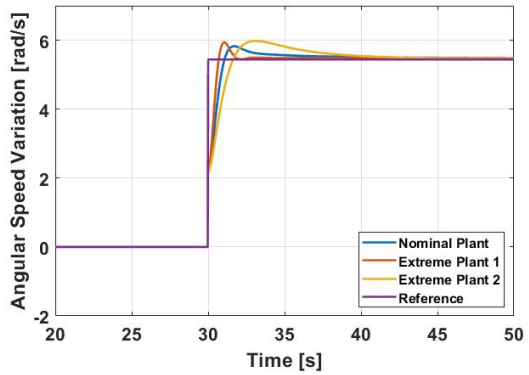

Figure 10: Angular Speed Variation

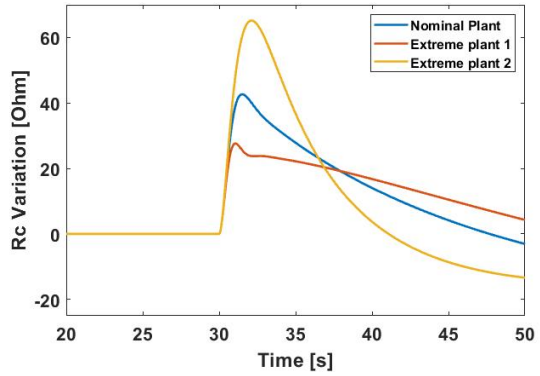

Figure 11: Control Effort

The effect on the TSR of the abrupt increase of the wind speed is presented in Figure 12.

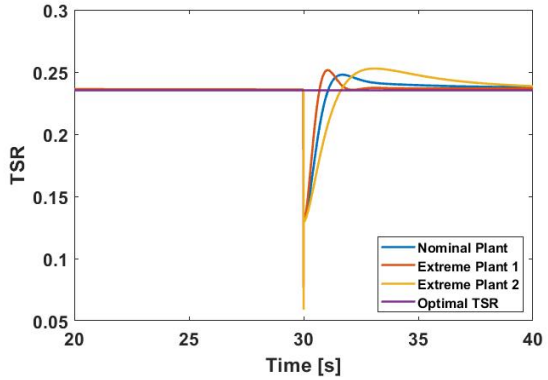

Figure 12: Tip Speed Ratio

The sudden change in the wind velocity causes a decrease in the TSR and consequently a decrease in the turbine's efficiency. The presence of the controller counteracts this effect, and in less than $10\,s$ the turbine's efficiency is again at its maximum.

6.2. With Turbulence

In order to test the conditions as real as possible, the step input was substituted for a smoother signal, and the turbulence present in a real wind stream was considered. The wind value from which is computed the optimal angular speed, is still the signal without turbulence. Thus, the signal with turbulence will only be used as a disturbance, and not to compute the reference.

The wind input is modelled resorting to the turbulent wind model presented before. After the addition of the turbulence model, the wind speed signal is as presented in Figure 13.

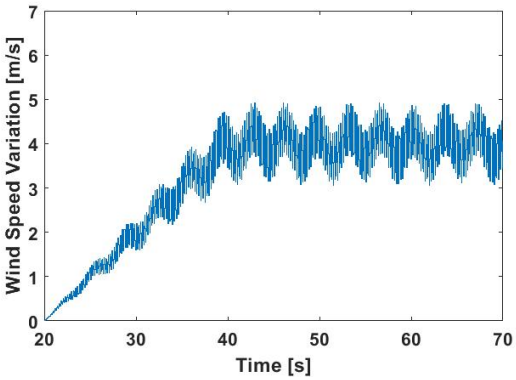

Figure 13: Wind Speed Variation with Turbulence

For a cleaner observation, this simulation is only shown for the nominal plant, as the results from the three plants are lookalike, and overlap each other.

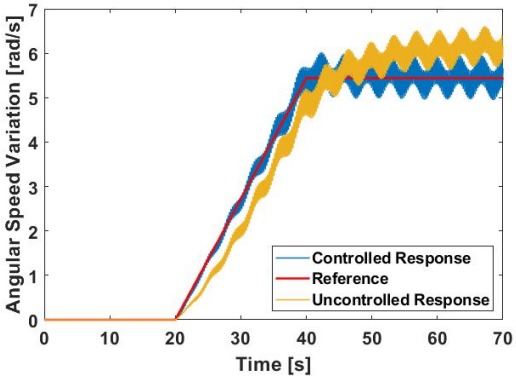

Figure 14: Angular Speed Variation

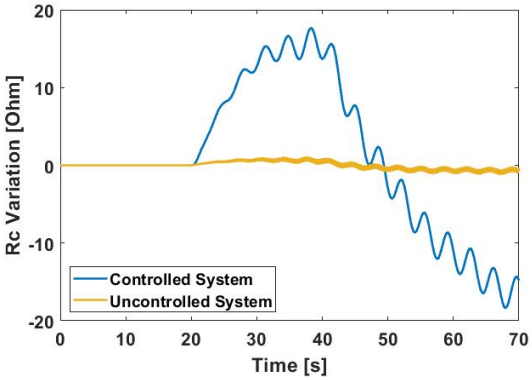

Figure 15: Control Effort

In Figure 14 it is shown that despite the turbu-

lence and the variation around the optimal angular speed, the system can track reasonably well the reference imposed by the variation of $4\,\mathrm{m/s}$ in the wind speed. The circuit imposed load has its maximum value of approximately $151\,\Omega$ for a $\Delta R_c \approx 15\,\Omega$. The comparison between the optimal TSR value, and the achieved one is presented in Figure 16.

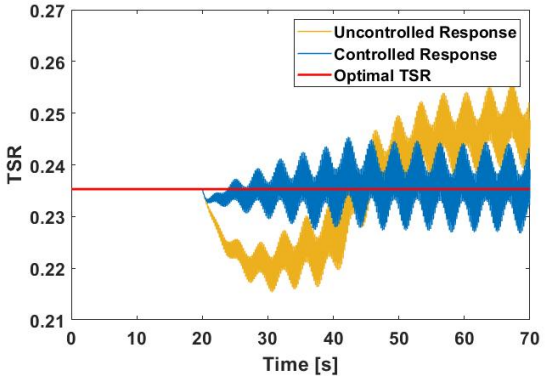

Figure 16: Tip Speed Ratio

It is obvious that there is an improvement when using the CRONE control. While the controlled response oscillates around the optimal TSR, the uncontrolled one is almost always far from the optimal point.

6.3. Controller Performance Assessment

In order to evaluate the performance of the controller the following metrics were applied:

- the integral of time multiplied by the absolute value of the error (*ITAE*):

$$ITAE = \int_0^f t \cdot |e(t)|\, dt \tag{13}$$

- integral of the square value (*ISV*) of the control input:

$$ISV = \int_0^f u^2(t)\, dt \tag{14}$$

where *ITAE* is used as a numerical measure of tracking performance for the entire error curve, and *ISV* show the energy consumption of the control effort.

As in the case where the wind turbulent model is used, only appears turbulence from $20\,s$ on, the time frame taken into account is from 20 to 70 seconds for the simulation with turbulent wind input. In the step input, only the simulation occurred after the step will be analysed. Tables 3 to Table 4 summarise the performance assessment results for the different simulations.

As expected, the step input simulation without turbulence is the easiest test to track, as the reference signal is simple and does not include any disturbances other than the wind step itself. However, is the test that requires a greater energy consumption, as the high amplitude abrupt change in the reference, has to be accompanied by a higher control effort.

In both tests, again as it was expected, the *ITAE* results are much better for the controlled system when compared to the closed-loop uncontrolled system.

When comparing the results between plants, one can observe that the difference from the plant with the higher *ITAE*, to the one with the lower, is small, within the same test and for the controlled response. This particularity highlights the capability of the third generation CRONE controller in positioning the uncertainty domains, in such a way that they have the smallest influence in the system's behaviour.

7. Experimental Setup

The necessity to measure and manipulate physical quantities is common to all control and identification problems that move, beyond simulation, into the real world.

7.1. Angular Speed Sensor

For the angular speed measurement the choice was to use an infrared optical sensor.

The solution used consists in using a reflective infrared optical sensor, in which the emitter and the photoresistor are parallel to each other. In this situation, the photoresistor only receives a signal when an object passes at a limited distance in front of the sensor. In this type of setup there is no need for coupling another structure to a turbine's blade, and a higher precision can be achieved without increasing the number of structures to interrupt the beam, as the object in which the infrared beam is reflected can be each blade support. The solution adopted is represented in Figure 17.

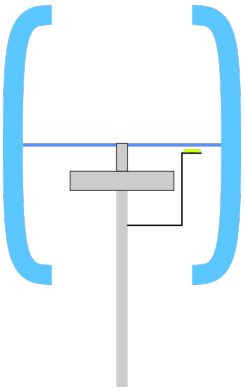

Figure 17: New Angular Speed Sensor Setup

The infrared sensor included in this project has a range from 2.5 to $10\,\mathrm{mm}$, therefore there is enough clearance for the turbine's vibrations and looseness to occur without damaging the sensor.

Table 3: Step Input Simulation

	Nominal		Extreme 1		Extreme 2	
	$Uncontrolled$	$Controlled$	$Uncontrolled$	$Controlled$	$Uncontrolled$	$Controlled$
ITAE	797.594	27.76	802.747	32.133	796.198	19.855
ISV	38.702	14731	35.853	10102	39.439	22716

Table 4: Harmonic Turbulent Wind Simulation

	Nominal		Extreme 1		Extreme 2	
	$Uncontrolled$	$Controlled$	$Uncontrolled$	$Controlled$	$Uncontrolled$	$Controlled$
ITAE	695.116	265.064	694.251	256.437	698.469	271.769
ISV	17.129	6447.1	16.93	4680	17.368	8715.3

To secure the new infrared sensor in position, an aluminium support was built. The sensor has three pins, Vcc, GND and $Signal$. These pins are connected to $5V$, $Ground$ and digital pin 3 in the *Arduino* respectively. It makes use of the *Arduino* function *interrupts()* specific for these cases when one cannot be dependent of the sampling time to catch the interruptions on the sensor.

7.2. Wind Speed Sensor

The hardware chosen to measure this physical quantity was a cup anemometer, commercialised by *SparkFun* as part of weather station *kit*. The anemometer makes use of a reed switch and a neodymium magnet, that closes the switch two times per revolution. Knowing the time between clicks, it is possible to compute the angular velocity of the anemometer.

In the distributor's website, a guide can be found where is announced that, for this specific equipment: $1\ Rev/sec = 2.4\ \mathrm{km/h} = 0.666\ \mathrm{m/s}$. Resorting to this conversion factor, the incident wind speed can be trivially computed.

7.3. Actuators

In order to implement the control strategy, an automated way to manipulate the control variable Rc was implemented. The solution found was to attach one servo motor to each rheostat (Figure 18). This is not an ideal solution, as the rotational range of the servo motor is shorter than the rheostat's. Instead of the original range from 0 to $100\,\Omega$ the actuator's range becomes limited from 0 to $80\ \Omega$. As a matter of versatility and to allow tests to be made with the PMSG in open-circuit, a relay module was included. This device is a set of *Arduino* controlled switches, enabling the simulation of $Rc = inf$.

Being the generator a 3-phase PMSG, the resistive loads are mounted in a Delta configuration.

The servo motors have 3 wires, *Black*, *Red* and *White*. These stand for *Ground*, *5V* and *Signal* respectively. These standard servo motors are controlled by *Arduino* resorting to *PWM* (Pulse Width Modulation), feature of some digital pins.

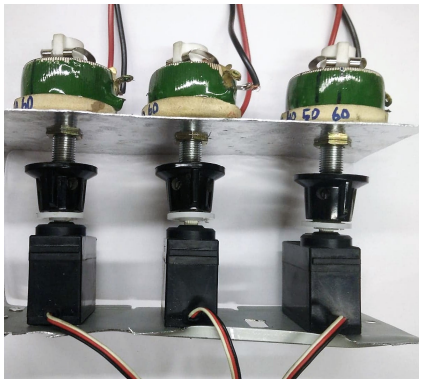

Figure 18: Servo Motors and Rheostats Structure

8. Experimental Results

Two tests in open loop were performed. The first test was intended to evaluate the prototype's TSR range, and to compare it to the maximum value proposed in section 2. The second test, intended to evaluate the minimum and maximum TSR that could be achieved when using the actuators developed. The purpose of these tests is to get to know the prototype's limits for control design purposes, and to have an idea of what rheostats to use when designing future actuators.

For both tests are presented, the raw data acquired from the sensors, and the low-pass filtered data.

8.1. Open-Loop Test Without Rheostat

This first test begins with the PMSG in open-circuit, and, at $t = 200\,\mathrm{s}$, the circuit is closed. The wind stream was kept at a constant speed of around $6\,\mathrm{m/s}$ for the entire test. The results for the rotor angular speed obtained in this first test are presented in Figure 19.

In figure 19 it can be seen that, in open-circuit, the turbine takes almost $100\,\mathrm{s}$ to reach the steady state angular speed, presenting a small overshoot. Once in steady state, the rotor angular speed can be seen as constant, around $\omega = 11.5\,\mathrm{rad/s}$.

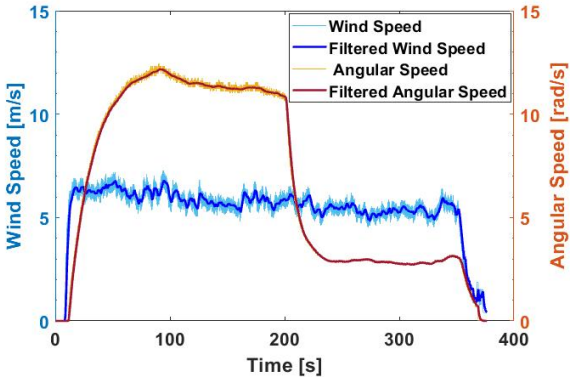

Figure 19: Wind Speed vs Rotor Angular Speed

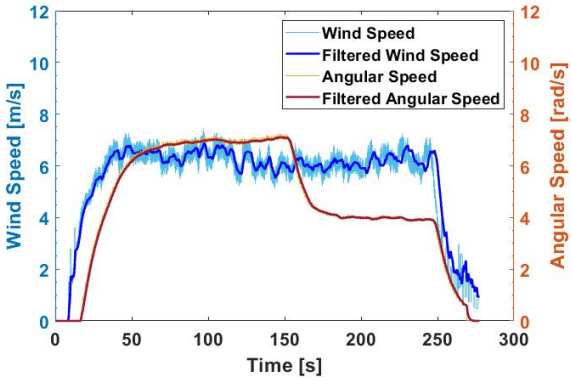

Figure 21: Anemometer Signal

When the circuit is closed, the angular speed drops $8.5\,\mathrm{rad/s}$, to around $3\,\mathrm{rad/s}$. The TSR evolution along this first test is presented in Figure 20.

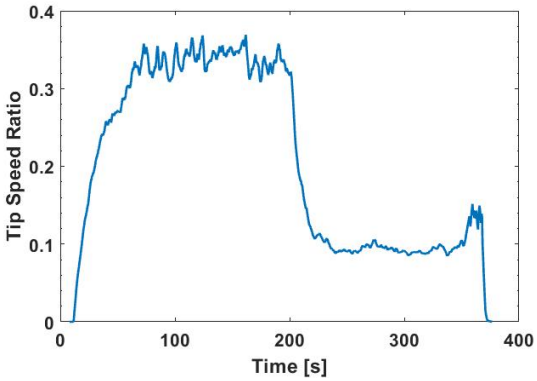

Figure 20: TSR- Open-Circuit vs Short-Circuit

The results obtained in this test, are consistent with theoretical results from section 2. The maximum tip speed ratio presented by the prototype is around 0.35 in open-circuit. The minimum TSR, obtained with the PMSG in short-circuit, is around 0.1. Placing the steady state TSR in the $[0.1; 0.35]$ interval.

8.2. Open-Loop Test With Rheostat

In this second test, the objective was to assess the TSR range available when introducing the rheostats as actuators. The variable resistances installed have an actuation range of 80Ω, from 0 to 80Ω.

The present test was conducted similar to the previous one, the wind speed was increased to approximately $6\,\mathrm{m/s}$, and kept at that value until $t = 250\,\mathrm{s}$. The resistance is at $80\,\Omega$, from the beginning of the test until $t = 150\,\mathrm{s}$, when it is changed for $0\,\Omega$ until the end of the test. The wind speed and rotor angular speed values are presented in Figure 21.

The results show that the angular speed, when the actuator is in the upper limit of its range, is smaller in $5.5\,\mathrm{rad/s}$ when compared with the test in open-circuit. The low wind self-start capability, is also compromised. The prototype initiates its movement for a higher wind speed than in the first test. In Figure 22 is presented the TSR evolution that resulted from this test. The tip speed ratio obtained in this second test, has a maximum value of approximately 0.2, contrasting with the value of 0.35 obtained in the first test. The minimum value is again placed around 0.1, as the smallest resistance value of $0\,\Omega$ was kept constant between tests. The small range presented by the rheostat installed limits the prototype's TSR to less than half its range. For control purposes, a larger actuation range provides more room to manipulate the turbine's behaviour. Therefore, in a future implementation, rheostats with a higher range should be installed.

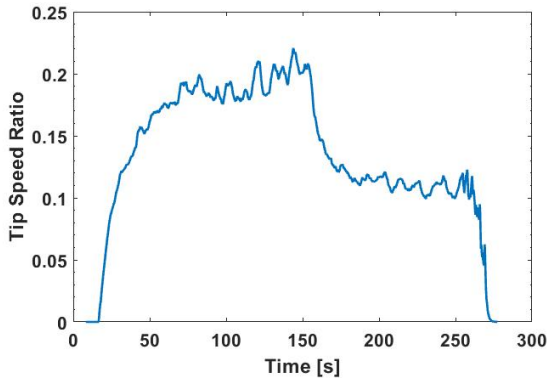

Figure 22: Anemometer Signal

9. Conclusions

In this document a Darrieus VAWT prototype is studied. Real and simulation data from previous projects are analysed, and considerations are made. It was proven that the maximum tip speed ratio possible to be achieved by this prototype, with this PMSG, is around 0.353; far from the $\lambda_{opt} = 7$, used in previous work.

Five models developed in [6] were analysed, the one that presents a response closer to the pro-

totype's behaviour, is presented and selected for control development. The selected MISO identified model was used as the nominal plant that describes the prototype. $\pm 20\%$ of uncertainty in the transfer function's coefficient, was added to the model.

A fractional third generation CRONE control was successfully developed resorting to the CRONE CSD Toolbox.

Two different disturbances were used to test the controller in a simulation environment: a step and a modelled harmonic turbulent wind. In general, the controlled system has a tracking performance (*ITAE*), twice as good as the system's response without controller ($C = 1$). The CRONE controller has a good performance when it comes to overcome the differences between the nominal plant and perturbed one's. The metrics used to assess the controller performance do not present significant difference between plants, within the same test, despite the presence of the $\pm 20\%$ uncertainty in the controlled transfer function.

Experimental tests were performed, with the aim of confirming the prototype's TSR limits, obtained theoretically. Confirming the result obtained in section 2 for the maximum TSR of 0.35. Another test was conducted, to assess the limitations that the range of the actuator would impose to the behaviour of the prototype. This test led to the conclusion that, with the actuators installed, the range of the prototype's TSR would be reduced to less than half, from $[0.35; 0.1]$ to $[0.2; 0.1]$.

An effort should be done to obtain a new experimental $Cp(\lambda)$ curve, and a new theoretical model should be developed, based on this new curve. A new platform with more memory should be acquired to implement the control loop and test not only the controller developed in the present document, but also to compare it with the controllers developed in [6]. For this new implementation, the servo-motors should be replaced by stepper-motors and the rheostats replaced by ones with a wider range, or, instead, a digital potentiometer should be used.

References

[1] GWEC. Global wind report - anual market update. Technical report, Global Wind Energy Council, 2017.

[2] N. C. Batista, R. Melício, V. M. F. Mendes, M. Calderón, and A. Ramiro. On a self start darrieus wind turbine; blade design and field tests. *Renewable and Sustainable Energy Reviews*, 52:508–522, Dec 2015. doi: 10.1016/j.rser.2015.07.147.

[3] N. Batista. *Novo Aerogerador de Eixo Vertical Integrado Numa Rede Inteligente em Contexto Urbano*. PhD thesis, Universidade de Évora, 2013.

[4] N. Batista, R. Melício, J. C. O. Matias, and J. P. S. Catalão. New Blade Profile for Darrieus Wind Turbines Capable to Self Start. pages 1–5. IET Conference on Renewable Power Generation (RPG 2011), Sept 2011. doi: 10.1049/cp.2011.0219.

[5] N. Batista, R. Melicio, and V. Mendes. Darrieus-type vertical axis rotary-wings with a new design approach grounded in double-multiple streamtube performance prediction model. 2018.

[6] T. Pereira, N. Batista, A. Fonseca, C. Cardeira, P. Oliveira, and R. Melicio. Darrieus wind turbine prototype: Dynamic modeling parameter identification and control analysis. *Energy*, 159:961–976, Sep 2018. doi: 10.1016/j.energy.2018.06.162.

[7] A. Oustaloup. La Commande CRONE. *Commande Robuste d'Ordre Non Entier*, (6):130–135, 1991.

[8] P. Lanusse, A. Oustaloup, and B. Mathieu. Third generation CRONE control. In *Proceedings of IEEE Systems Man and Cybernetics Conference - SMC*, pages 149–155. IEEE, 1993. doi: 10.1109/ICSMC.1993.384864.

[9] P. Lanusse, R. Malti, and P. Melchior. CRONE control system design toolbox for the control engineering community: tutorial and case study. *Philosophical Transactions of the Royal Society*, (371), Apr . doi: 10.1098/rsta.2012.0149.

[10] F. Balduzzi, A. Bianchini, E. A. Carnevale, L. Ferrari, and S. Magnani. Feasibility analysis of a Darrieus vertical-axis wind turbine installation in the rooftop of a building. *Applied Energy*, 97:921–929, Sept 2012. doi: 10.1016/j.apenergy.2011.12.008.

[11] R. Melício. *Modelos Dinâmicos de Sistemas de Conversão de Energia Eólica Ligados à Rede Eléctrica*. PhD thesis, Universidade da Beira Interior, 2010.

[12] J. Sabatier, P. Lanusse, P. Melchior, and A. Oustaloup. *Fractional Order Differentiation and Robust Control Design*, volume 77 of *Intelligent Systems, Control and Automation: Science and Engineering*. Springer Netherlands, 2015. ISBN 978-94-017-9806-8.